Facile synthesis and electrochemical properties of Prussian Blue/MWCNT and PB/WO$_3$ films

E. Yakar

Department of Materials Science and Engineering, Faculty of Engineering, Çanakkale Onsekiz Mart University, Çanakkale, Turkey

In this study, Prussian Blue (PB)/MWCNTs and PB/WO$_3$ nanocomposite films were deposited onto In-SnO$_2$ (ITO) substrates by a simple chemical bath deposition method. The structural, morphological, and electrochemical properties of PB/MWCNTs films were systematically investigated in detail. Removing influence of ITO, it was evident that both of the patterns could be indexed in the cubic PB phase, from X-ray diffraction analysis. While intense tubular carbon and agglomerative formations were detected in PB/MWCNTs films, cubic PB and spherical WO$_3$ forms were depicted in PB/WO$_3$ films. Average particle sizes (D) of MWCNTs (5.8 nm) were smaller than WO$_3$ (10.5 nm) due to improved particle growth process as shown in this work. Raman analysis proved the production of PB structures. Typical Prussian Blue ν(CN) and stretching vibration of Fe-C at 2159 cm^{-1} and 507 cm^{-1} were observed, respectively. Improved electrochemical performance of PB/MWCNTs electrodes was indicated compared to PB/WO$_3$ electrodes.

INTRODUCTION

As a primary synthetic coordination compound, Prussian Blue (Fe$_4$[Fe(CN)$_6$]$_3$, PB) has been realized as an essential class of transition metal hexacyanides with its unique structure. With the increasing research interest and industrial need for electrochemical mediators, PB has found wide use in biosensors [1], electrochemical sensors [2], rechargeable batteries [3], electro-catalysts [4], and electrochromic devices [5]. In particular, researchers have explicated an intensified interest in the electrochemical activity of PB films due to the increasing demand for the integration of smart devices in our daily life. Although Prussian Blue has good oxidation/reduction properties with high electrochemical activity, the main challenge is the rapid degradation of electrochemical properties [6]. Because the PB layer has low stability where there is too much accumulation, chemical reaction kinetics can decrease between ferric chloride and ferricyanide ions [7]. To solve this problem, polymer matrix formation with PB analogues [8, 9], PB/C-based material nanocomposites [10, 11] and doping [12] processes have been preferred, using the advantage of structural designability and tunable redox potential of Prussian Blue.

On the other hand, unique physical and chemical properties of multi-walled carbon nanotubes (MWCNTs) have afforded developing new promising functional nanocomposites by exposing numerous functional groups at the end of tubes [13, 14]. Several studies have reported enhanced electrochemical performance of PB after modification with MWCNTs. Li *et al.* showed that the introduction of MWNTs resulted in improved electrochemical stability and enhanced response current to reducing hydrogen peroxide (H$_2$O$_2$) of the PG/PB electrode [15]. According to our previous study, the MWCNTs coating on PB/ZnO film yielded an enormous impact on its electrochemical properties by increasing defect sites [16]. Vieira *et al.* explained that the heterogeneous reaction between the electrolyte and iron species led to the formation of PB particles, and their decreasing sizes resulted in better interactions with MWCNTs depending on the scan rate. (10 and 100 mV s^{-1}) [17]. Boron [18], lanthanide [19], and zinc [20] ions were doped on PB films, which were utilized as H$_2$O$_2$ electrochemical sensors and in photothermal applications. Due to its structural transformations, substoichiometric phase transitions and good electrochemical properties, tungsten oxide was selected in this study [21].

Although some researches have been carried out on the modification of PB films with nanoparticles, there is very little scientific understanding of the impact of MWCNTs and WO$_3$ with various physical properties and morphologies on the electrochemical performance of PB films. The aim of this paper is to critically analyze the impact of the PB films of MWCNTs and WO$_3$ on their electrochemical performance and to address possible nano- and microscale mechanisms

contributing to their electrochemical properties. A facile chemical bath deposition method was used to the preparation of films. Different characterization techniques were utilized to reveal their structural, morphological and electrochemical properties.

EXPERIMENTAL

PB/MWCNT and PB/WO$_3$ films were prepared by a simple chemical bath deposition method onto In-doped SnO$_2$ (ITO) substrates. First, ITO substrates were cleaned by an aqueous solution mixed with ethanol and acetone in ultrasonic bath. Fe$_2$(SO$_4$)$_3$ (Sigma Aldrich, 97%), K$_4$[Fe(CN)$_6$]$_3$ H$_2$O (Sigma Aldrich) and HCl (30 %) were used for the preparation of PB films employing a modified synthesis reported in [22]. MWCNTs (0.02 g) purchased from Nanografi, Turkey (diameters about 20–30 nm and average length of 1.5 μm) was mixed with Fe$_2$(SO$_4$)$_3$ solution on a magnetic stirrer for 30 min to obtain PB/MWCNT films. In addition, 0.1 M Na$_2$WO$_4$.2H$_2$O was added to K$_4$[Fe(CN)$_6$] aqueous solution to obtain PB/WO$_3$ films. Both films were annealed at 150 ºC for 2 h to remove surface contaminations.

Characterization

All characterizations were realized at room temperature. The structural composition and structural parameters were investigated by X-ray diffraction (XRD) analysis by Rigaku SmartLab X-ray diffractometer with CuK$_\alpha$ (1.5406) which was operated at 45 KV and 40 mA. Average particle size (D), dislocation density (δ) and microstrain (ε) were measured by the equations given below:

D= 1.5406/ β cosθ   (Equation 1)

δ= 1/D^2 (Equation 2)

ε= β/ 4 tan θ   (Equation 3)

Surface morphology of the PB/MWCNT and PB/WO$_3$ films was depicted by JEOL JSM-7100 F SEM scanning electron microscope. To characterize the electrochemical properties of these films, cyclic voltammetry (CV) and electrochemical impedance spectroscopy (EIS) measurements were carried out. Electro-activity of the samples was determined by a standard three-electrode configuration (Electrochemical Compactstat Interface/ Ivium Page Technologies) with reference electrolyte type and the scan rate was chosen as 5 mM (Fe(CN)$_6$)$^{3-/4-}$/KCl and 50 mV/s. For the three-electrode configuration,

working electrode, counter electrode and reference electrode were ITO, BASI Pt wire and BASI Ag/AgCl, respectively. Impedance curves were obtained using a Compactstat Interface (Ivium Technologies-Eindhoven/ The Netherlands) and Autolab PGSTAT 128N potentiostat/galvanostat equipped with a FRA2 frequency response analyzer. Raman spectra of the films were recorded by Thermo DXR Raman spectrophotometer, exciting 780 nm laser line in the wavenumber range between 100-3000 cm^{-1}.

RESULTS AND DISCUSSION

Structural analysis

XRD patterns of the films in the range of 2θ = 20-80º are shown in Fig. 1. Both films displayed a polycrystalline structure. Three weak ITO-based peaks were identified in the range of 2θ = 50-70º, indicating that both films adhered well to the substrate. Both samples exhibited different PB corresponding peaks in the range of 2θ = 15-40º, which could be assigned to JCPDS Card No:73-0687 [23]. PB/MWCNTs samples showed characteristic carbon peaks as C(002) and C(100) at 2θ = 25.6º and 2θ = 43.2º, respectively [24]. Beside, PB/WO$_3$ samples had preferential orientation at 2θ = 31.8º, corresponding to the orthorhombic WO$_3$ (220) phase [25]. These results suggested that complex polycrystal forms were obtained [26]. Average particle sizes (D) of MWCNTs were smaller than those of WO$_3$ due to improved particle growth process as shown in Table 1 [27].

Surface Morphology

Surface morphology of the PB nanocomposite films is represented in Fig. 2. In general, crack-free film formations were observed for both films and relatively homogeneous film surface was confirmed. PB/MWCNTs sample surface was covered by tubular structures with different lengths and similar diameters. Partial cluster formations were also obtained due to PB particle growth process. Tubular forms provide a 3D-network that aids to decrease electrical resistance in in-plane and thorough thickness directions, therefore the electrode efficiency of the resulting structure could be increased [28]. On the other hand, it has been observed that PB nanocubes with side length between 50 to 100 nm and WO$_3$ nanospheres as a heterostructure form were obtained in PB/WO$_3$ films [26].
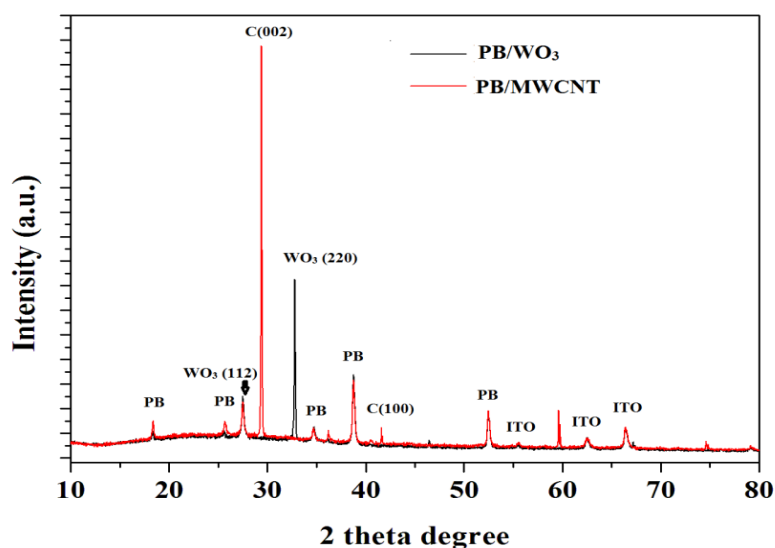
Fig. 1. XRD patterns of PB/MWCNT and PB/WO₃ films

Table 1. Structural parameters of PB/MWCNT and PB/WO₃ films

	2θ (º)	FWHM (rad)	d (Å)	D (nm)	Dislocation density (δ)	Microstrain (ε)
PB/MWCNT	32.7	0.0016	2.730	5.8	0.029	0.000110
PB/WO₃	29.3	0.0010	3.036	10.5	0.009	0.000089
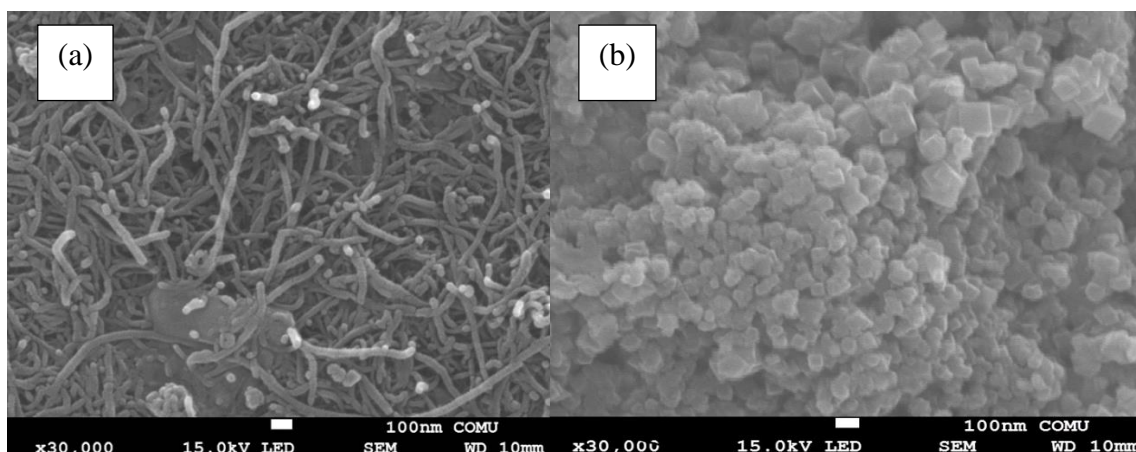
Fig. 2. SEM images of a) PB/MWCNT and b) PB/WO₃ thin films

Electrochemical Characterization

The electrochemical performance of PB/MWCNTs and PB/WO₃ electrodes was investigated by cyclic voltammetry in 5 mM $K_3[Fe(CN)_6]$, $K_4[Fe(CN)_6] \cdot 3H_2O$ in KCl including redox couple solution at a scan rate of 50 mV/s as represented in Fig. 3. Higher anodic and cathodic response was observed in PB/MWCNT electrode compared to PB/WO₃ electrode. The cathodic response was higher than the anodic response for both samples, as shown in Table 2 due to the lack of proper lattice coordination of iron ions. The reversible conversion cycle was determined between -1 V (-0.9 V) and 1 V (0.8 V) for PB/MWCNTs nanocomposite PB/WO₃ electrode that indicated an increased electrochemical stability effect on PB [29]. These results showed that along with the large surface area provided by MWCNTs, it provides enhanced Fe-carboxyl-CN interactions compared to Fe^{3+}-W^{6+} ions interactions on the

electrode surface [30]. To investigate the charge-transfer process at the electrode/solution interface, electrochemical impedance spectroscopy (EIS) is a powerful tool.
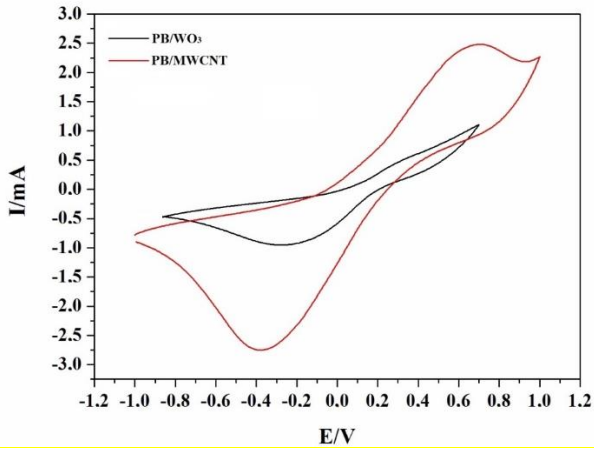
Fig. 3. Cyclic voltammogram of PB/MWCNT and PB/WO₃ electrodes in background solution (5 mM K₃[Fe(CN)₆], K₄[Fe(CN)₆].3H₂O in KCl) at an optimum scan rate of 50 mV/s

In the range between 0.10 Hz and 10^5 Hz, Nyquist plots of PB/MWCNTs and PB/WO₃ nanocomposite electrodes are shown in Figs. 4(a) and 4(b), respectively; fitting the electric model presented in Fig. 4(c). The impedance behavior of the electrodes was different and showed a high semicircle diameter for both electrodes with 5 mM KCl supporting electrolyte solution. The R_{ct} (Ω) values indicated an improvement in the conductivity by WO₃ implementation of PB when compared to MWCNTs coating in PB [31]. Warburg line extrapolation in the low frequency's limit is the double layer capacitance at the ITO/sample interface and no serious differences were seen for both electrodes, indicating that the diffusion process was relatively improved by W^{6+} ions and conductive MWCNTs coating [32].

Raman spectra of PB/MWCNTs and PB/WO₃ nanocomposite films are shown in Fig. 5. Typical Prussian Blue ν(CN) and stretching vibration of Fe-C at 2159 cm⁻¹ and 507 cm⁻¹ are observed, respectively. ν(CN) band of PB/WO₃ appears sharper and with higher intensity compared to the PB/MWCNTs nanocomposite films, indicating improved crystallization [33]. The agglomerated ferricyanide ion bands appeared at 1200 cm⁻¹ [34]. Both MWCNT- and WO₃- related bands are not observed due to their low concentration for interacting Prussian Blue particles.

Table 2. CV and EIS measurement results (R_{ct}: Charge transfer resistance; E^o: Formal potential)

Electrode	EIS Analysis	CV Response in 5.0 mM Fe(CN)₆³⁻/⁴⁻				
	R_{ct} (Ω)	E_a (V)	E_c (V)	E^o (V)	I_a (µA)	I_c (µA)
PB/WO₃	888	0.315	-0.275	0.295	2.5	745
PB/MWCNT	1956	0.685	-0.380	0.533	850	2413
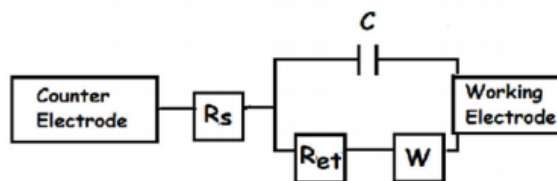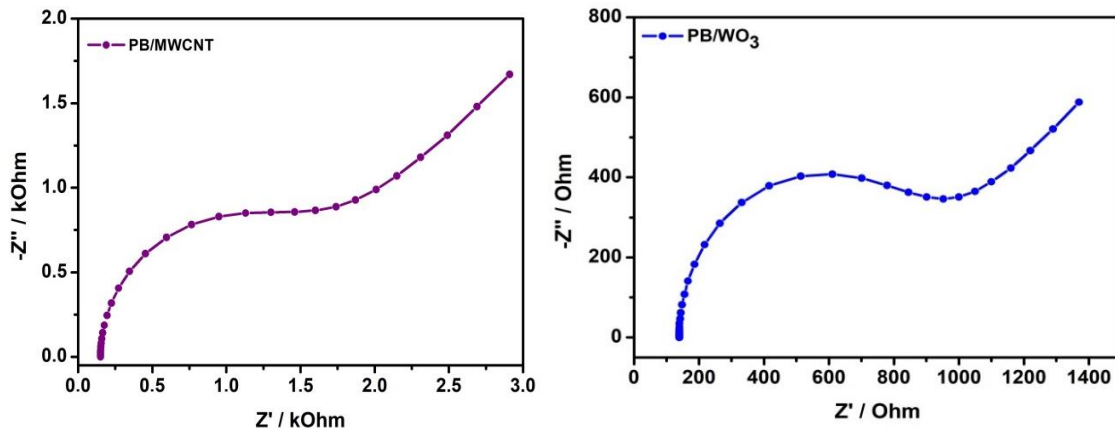
Fig. 4. Nyquist plots a) PB/MWCNT; b) PB/WO₃ with redox couple; c) electric model
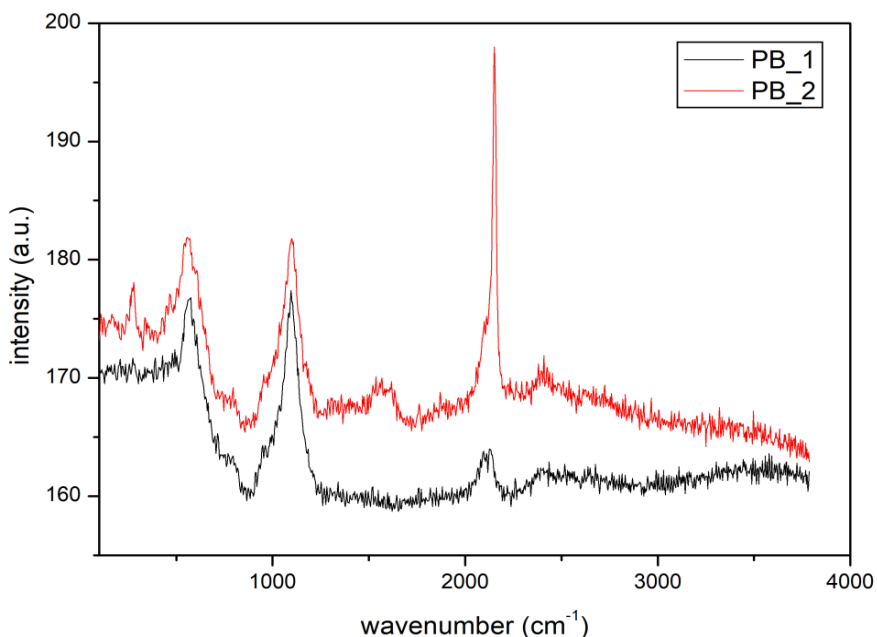
Fig. 5. Raman spectrum of PB/MWCNT (PB_1) and PB/WO₃ (PB_2) films

CONCLUSION

In this study, PB/MWCNTs and PB/WO₃ structures were successfully synthesized by the chemical bath deposition method on electrically conductive In-doped SnO_2 substrates. The intense X-ray patterns were narrow and sharp indicating that Prussian Blue was well crystallized. SEM images showed various types of PB morphologies with different sizes (tubes, cubes and clusters) in both films. Upon redox cycling, PB/MWCNTs nanocomposite electrodes in a wider potential range were electrochemically more stable than PB/WO₃ electrodes. From these results it may be concluded that MWCNTs would be an appropriate nanocomposite part for PB-based electrochemical devices.

REFERENCES

1. N. Ç. Kurt, M. S. Çelebi, *Ordu Univ. J. Sci. Tech.*, **1**, 31 (2018).
2. M. D. J. Masaquiza, L. Fernández , G. González, *Nanomaterials*, **10**, 1328, (2020).
3. B. Huang, Y. Shao, Y. Liu, Z. Lu, X. Lu, S. Liao, *CS Appl. Energy Mater.*, **2**(9), 6528 (2019).
4. Y. Feng, X. Wang, P. Dong, J. Li, L. Feng, J. Huang, L. Cao, L. Feng, K. Kajiyoshi, C. Wang, *Scientific Reports*, **9**, 15965 (2019).
5. A. Takahashi, K. Noda, H. Watanabe, T. Kawamoto, *RCS Advances*, **9**, 40183 (2019).
6. K. Hurlbutt, S. Wheeler, I. Capone, M. Pasta, *Joule,* **2**, 1 (2018).
7. F. Doroftei, T. Pinteala, A. Arvinte, *Microchim. Acta,* **181,** 111 (2014).
8. L. Wu, T. Pang, Y. Guan, Y. Li, *Polymers,* **11**, 266 (2019).
9. L. V. Lukachova, E. A. Kotelnikova, D. D'Ottavi, E. A. Shkerin, E. E. Karyakina, D. Moscone, G. Palleschi, A. Curulli, A. A. Karyakin, *IEEE Sensors Journal*, **3**, 3 (2003).
10. M. Chen, Z. Zhang, X. Liu, Y. Li, Y. Wang, H. Fan, X. Liang, Q. Chen, *RSC Advances*, **10**, 31773 (2020).
11. S. Husmann, S. G. Booth, A. G. J. Zarbin, R. A. W. Dryfe, *J. Braz. Chem. Soc.,* **29**(5), 1130 (2018).
12. Y. Zhu, Z. Zhang, J. Bao, S. Zeng, W. Nie, P. Chen, Y. Zhou, Y. Xu, *Int. J. Energy Res.,* **44**, 9205 (2020).
13. K. K. Gangu, S. Maddila, S. B. Jonnalagadda, *Science of the Total Environment*, **646**, 1398 (2019).
14. E. Moaseri, M. Karimi, M. Maghrebi, M. Baniadam, *Science of the Total Environment*, **51** 774 (2014).
15. Z. Li, J. Chen, W. Li, K. Chen, L. Nie, S. Yao, *Journal of Electroanalytical Chemistry,* **603**, 59 (2007).
16. F. Ozutok, E. Yakar, *Journal of New Materials for Electrochemical Systems,* **21**, 119 (2018).
17. T. A. Vieira, J. R. Souza, D. T. Gimenes, R. A. A. Munoz, E. Nossol, *Solid State Ionics*, **338** 5 (2019).
18. M. A. Komkova, A. Pasquarelli, E. A. Andreev , A. A. Galushin, A. A. Karyakin, *Electrochimica Acta*, **339**, 135924 (2020).
19. X. Chena, G. Wua, J. Tanga, L. Zhou, S. Weia, *Inorganic Chemistry Communications*, **114**, 107821 (2020).
20. J. Li, X. Liu, L. Tan, Z. Cui, X. Yang, Y. Liang, Z. Li, S. Zhu, Y. Zheng , K. W. K. Yeung, X. Wang, S. Wu, *Nature Comminications,* **10**, 4490 (2019).
21. K. Rong, H. Zhang, H. Zhang, Y. Hu, Y. Fang, S. Dong, *ACS Appl. Electron. Mater.*, **1**, 1038 (2019).

22. J. Velevska, M. Pecovska-Gjorgjevich, N. Stojanov, M. Najdoski, *IJSBAR*, **25**(3), 380 (2016).
23. N. Ghasdian, Y. Liu, R. McHale, J. He, Y. Miao, X. Wang, *J. Inorg. Organomet. Polym.*, **23**, 111 (2013).
24. T. Arunkumar, R. Karthikeyan, R. Ram Subramani, K. Viswanathan, M. Anish, *International Journal of Ambient Energy,* **41**(4), 452 (2020).
25. S. Zhuiykov, E. Kats, *Nanoscale Research Letters*, 9, 401 (2014).
26. S. Tadano, B. Giri, *Science and Technology of Advanced Materials,* 12, 064708, (2011).
27. K. H. Bhuiyan, M. Rahman, F. Mina, M.R. Islam, A. Gafur, A. Begum, *Composites: Part A,* **52,** 70 (2013).
28. Y. Yao, X. Bai, K. K. Shiu, *Nanomaterials*, **2**, 428 (2012).
29. N. S. Pham, Y. H. Seo, E. Park, T. D. D. Nguyen, I. S. Shin, *Electrochimica Acta*, **353**, 136446 (2020).
30. L. M. N. Assis, R. C. Sabadini, L. P. Santos, J. Kanicki, M. Łapkowski, A. Pawlicka, *Electrochimica Acta*, **182**, 878 (2015).
31. M. Saravanan, M. Ganesan, S. Ambalavanan, *RSC Advances*, **5**, 26081 (2015).
32. H. Fu, C. Liu, C. Zhang, W. Ma, K. Wang, Z. Li, X. Lu, G. Cao, *J. Mater. Chem. A*, **5**, 9604 (2017).
33. G. Moretti, C. Gervais, *J. Raman Spectrosc.*, **49**, 1198 (2018).
34. F. Grandjean, L. Samain, G. J. Long, *Dalton Trans.*, **45**, 18018 (2016).